Physical Biology

NOTE

Multivalent molecular tension probes as anisotropic mechanosensors: concept and simulation

To cite this article: Aaron T Blanchard and Khalid Salaita 2021 *Phys. Biol.* **18** 034001

Physical Biology

NOTE

Multivalent molecular tension probes as anisotropic mechanosensors: concept and simulation

Aaron T Blanchard[1,*] and Khalid Salaita[1,2]

[1] Wallace H. Coulter Department of Biomedical Engineering, Georgia Institute of Technology and Emory University, Atlanta, GA 30322, United States of America
[2] Department of Chemistry, Emory University, Atlanta, GA 30322, United States of America
[*] Author to whom any correspondence should be addressed.

E-mail: ATBlanchard@ymail.com and k.salaita@emory.edu

RECEIVED
25 October 2020

REVISED
8 December 2020

ACCEPTED FOR PUBLICATION
14 December 2020

PUBLISHED
10 March 2021

Keywords: mechanosensor, DNA nanotechnology, DNA mechanotechnology, TCR, integrin, multivalency

Abstract

Cells use protein-based mechanosensors to measure the physical properties of their surroundings. Synthetic tension sensors made of proteins, DNA, and other molecular building blocks have recently emerged as tools to visualize and perturb the mechanics of these mechanosensors. While almost all synthetic tension sensors are designed to exhibit orientation-independent force responses, recent work has shown that biological mechanosensors often function in a manner that is highly dependent on force orientation. Accordingly, the design of synthetic mechanosensors with orientation-dependent force responses can provide a means to study the role of orientation in mechanosensation. Furthermore, the process of designing anisotropic force responses may yield insight into the physical basis for orientation-dependence in biological mechanosensors. Here, we propose a DNA-based molecular tension sensor design wherein multivalency is used to create an orientation-dependent force response. We apply chemomechanical modeling to show that multivalency can be used to create synthetic mechanosensors with force response thresholds that vary by tens of pN with respect to force orientation.

1. Introduction

Mechanosensor proteins help transduce mechanical information into biochemical information by undergoing force-induced conformational changes [1]. These proteins are critical to cellular function, as they allow cells to physically respond to and interact with surrounding tissues and neighboring cells. Broadly speaking, mechanosensors play a pivotal role in mechanotransduction, wherein mechanical signals are converted to biomolecular and/or electrochemical signals. Some cell surface mechanosensors, such as the T-cell receptor (TCR) [2] and integrins [3], have been shown to behave as anisotropic mechanosensors that respond preferentially to pN force applied laterally to the cell membrane. We speculate that sensitivity to precise magnitudes of tension and force orientation can enhance the specificity of mechanosensation—a mechanism we describe as mechanical proofreading—for tasks such as the detection of foreign antigens and platelet aggregation [4]. Intracellular proteins such as vinculin have also been shown to utilize anisotropic mechanosensation to regulate processes such as directed migration [5].

The study of mechanosensor molecular biophysics has recently become more tractable due to the development of single molecule force spectroscopy (SMFS) [6] as well as molecular tension probes (MTPs) that generate a fluorescence signal in response to piconewton (pN) mechanical forces [7, 8]. In contrast to SMFS, MTPs enable mapping of the pN forces applied by individual mechanosensors in living cells. Existing MTPs do not respond in an orientation-dependent manner and are only sensitive to force magnitude. Hence, the development of MTPs that can respond in an orientation-dependent manner would enable testing of anisotropic mechanosensor models of receptor activation. More broadly, the ability to engineer anisotropic MTPs is an interesting challenge that may yield useful insight into biological function.

MTPs respond to pN-scale tension by extending to generate a fluorescence response. Our group designed and demonstrated the first MTPs, which were PEG polymers flanked with a fluorophore and quencher

pair and immobilized on a surface to detect forces transmitted by receptors such as EGFR [7] and the integrin adhesion receptor [8]. Over the past decade MTPs have been further engineered by our group and others using different proteins such as titin domains [9], and the spider silk motif [10], as well as polymers [11, 12], and nucleic acids [13]. The nucleic acid based probes have proven to be very powerful and facile to use and constitute the largest class of 'DNA mechanotechnology' tools that generate, sense, and transmit force [14]. Such tools have become critical to mechanobiology research and the development of force-generating nanomachines [15–17].

There are two major classes of DNA-based MTPs used in mechanobiology research. The first class, as presented by Xuefung Wang and Taekjip Ha [18] consists of short (∼25 bp) DNA duplexes called tension gauge tethers (TGTs). TGTs irreversibly rupture under force (figure 1(a)). These probes enable interrogation of the role of mechanical tension in receptor signaling by capping the maximum force exerted through receptor proteins at a well-defined tension tolerance (T_{tol}) 12–56 pN in magnitude [3, 15, 16, 18–29]. T_{tol}—defined as the constantly-applied force that leads to a 50% probability of rupture after 2 s—can be tuned from ∼12 pN to ∼56 pN by changing the geometry of the probe from 'unzipping mode' (figure 1(c)) to 'shear mode' (figure 1(d)). One means of optically measuring TGT rupture involves using an anchor strand linked to a fluorophore and a top strand linked to a quencher, such that duplex separation results in an increase in fluorescence [20] (figures 1(a)–(d)).

The second class of probe, originally developed in parallel in the research groups of Salaita and Chen [13, 30], consists of DNA hairpin sensors that reversibly unfold and refold in a force-dependent manner to enable direct visualization of forces using fluorescence microscopy. The $F_{1/2}$, which is the equilibrium force at which a reversible probe spends equal amounts of time in the opened and closed states, can be tuned in the 4–19 pN range by adjusting hairpin stem-loop sequence. TGTs preturb mechanosensor signaling and allow correlating cell signaling with the maximum force magnitude transmitted through a mechanosensor. Complementing this capability, reversible hairpin probes minimally alter mechanosensor signaling and are instead used to determine the innate forces transmitted through mechanosensors.

As these MTP DNA-probes have increased in use, their well-characterized biophysical properties have been leveraged to engineer functions that extend beyond simple magnitude quantification. For example, Brockman *et al* recently exploited specific properties of DNA-fluorophore interactions to develop a fluorescence polarization-based approach to estimate force orientation [31–33]. Ma *et al* developed a method for storing mechanical information

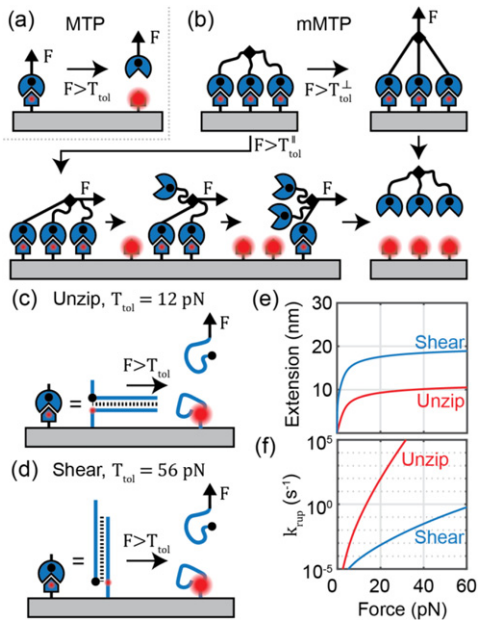

Figure 1. Concept and chemomechanical relationships. (a) An abstract representation of a TGT separating under force (***F***), resulting in dequenching of a fluorophore (red) due to separation from a quencher (black dot). (b) A multivalent TGT shown rupturing cooperatively due to force perpendicular to the surface exceeding $T_{tol}^{\perp}$ or noncooperatively due to force parallel to the surface exceeding $T_{tol}^{\parallel}$. (c) DNA depiction of high force (shear mode) and (d) low force (unzip mode) TGTs. (e) Force-extension curves for high force (blue) and low force (red) TGTs. For both probes, the duplex length is 25 basepairs and single stranded spacers are each 10 nucleotides. (f) Kinetic rate constants as a function of force for rupture (k_{rup}) of high force (blue) and low force (red) TGTs.

[34]. Murad and Li recently performed modeling that suggested that serially-connected TGTs could be used to overcome fundamental limitations of existing TGTs [35]. Forces between cells and between receptors on the same cell have been reported [36, 37]. We recently developed DNA origami-based tension probes that can simultaneously present multiple ligands and array up to three MTPs in parallel [38]. In that study, SMFS experiments and finite element analysis suggested that the DNA origami tension probes exhibited force-response thresholds that depended on force orientation, likely because force was unevenly transmitted to the MTPs. While the orientation-dependence was unexpected at the time, it encouraged us to consider the possibility of explicitly leveraging multivalency as a means of engineering anisotropic mechanosensation.

In this work, we use chemomechanical modeling to present a proposed design for MTPs that behave as anisotropic mechanosensors. We propose that multivalent MTPs (mMTPs), which consist of multiple MTPs linked in parallel to a single ligand-presenting 'body', will exhibit force thresholds that depend heavily on the orientation of force (figure 1(b)). This proposal hinges on (1) the dependence of total rupture force on the cooperativity between multiple

force-sensitive units linked in parallel, and (2) the dependence of cooperativity on pulling orientation. Evidence for (1) is borne out extensively within the SMFS-related literature [39]: when force is distributed evenly through multiple bonds, the force experienced by each individual bond is substantially reduced, thus resulting in a high collective rupture force; when force is concentrated onto one bond, then bonds will rupture sequentially and exhibit a total rupture force that is similar to the rupture force of a single bond. Evidence for (2) is borne out by force-balance principles, as well as specific literature examples [38]. Here, we only consider TGT-based mMTPs, although our findings bould also be applied to reversible DNA hairpin-based and non-DNA-based designs.

2. Approach

We modeled mMTPs using a chemomechanical model wherein probes are treated as nonlinear elastic springs that undergo force-dependent rupture transitions. An mMTP consists of a 'body' connected to N TGT 'springs'. One end of each spring is connected to the body and the other end is anchored to an underlying surface. The anchor points are uniformly distributed around the origin such that the position of the ith spring's anchor point is described, in x–y–z coordinates, as $[w\cos(i2\pi/N), w\sin(i2\pi/N), 0]$, where w is the width parameter (described below). In the absence of force the position of the body, $\boldsymbol{R}$, is $\boldsymbol{R} = [0, 0, 0]$. In the presence of force, $\boldsymbol{R}$ depends on the force orientation, which is defined by polar angle θ and azimuthal angle ϕ (figure 2(c)), such that $\boldsymbol{F} = |\boldsymbol{F}|[\sin(\theta)\cos(\phi), \sin(\theta)\sin(\phi), \cos(\theta)]$. In the presence of a force vector applied to the body, $\boldsymbol{R}$ is determined by energy balance principles; the total free energy of the mMTP (G) is defined by the energy associated with spring extension ($G_{\text{stretch},i}$). G can be represented as:

$$G = -\boldsymbol{F}\cdot\boldsymbol{R} + \sum_{i=1}^{N} G_{\text{stretch},i} \tag{1}$$

and $\boldsymbol{R}$ at equilibrium is determined by using gradient descent (specifically, MATLAB's fminunc function) to minimize G.

$G_{\text{stretch},i}$ is a monotonically increasing function of r_i, which is the end-to-end extension of the ith MTP. More specifically, $G_{\text{stretch},i}$ is calculated by integrating the force-extension curve of the spring with respect to r. In this work, we calculate the force-extension curve using an approximation of the worm like chain (WLC) model developed by Petrosyan [40] (more details are provided in supplemental note 3 of reference [15]). Force-extension curve calculations require the specification of (1) the number of segments per chain, (2) chain length per segment (h), and (3) persistence length (P). For low-force TGTs, we used a chain length of 20 single stranded DNA (ssDNA) nucleotides (nt) [18]. For high-force TGTs, we used a hybrid chain length consisting of 20 nt and 25 double stranded DNA (dsDNA) base pairs (bp) [18]. Based on literature estimates, we used $h = 0.34$ nm bp and $P = 53$ nm for dsDNA and $h = 0.66$ nm/nt and $P = 1.6$ nm for ssDNA. We calculated w by calculating the Boltzmann average extension from force extension curve at zero force:

$$w = \frac{\int \left(r\,\exp\left(-G_{\text{stretch}}\right) r^2\right) \mathrm{d}r}{\int \left(\exp\left(-G_{\text{stretch}}\right) r^2\right) \mathrm{d}r} \tag{2}$$

with the integrals taken from $r = 0$ to the contour length of the chain. These calculation yielded a w value of 4.6 nm for the low force TGT and 8.7 nm for the high force TGT.

An mMTP sensor with N force-sensitive units can exist in a total of 2^N possible states. For example: when $N = 1$, the single force-sensitive unit can either be folded or ruptured; when $N = 2$, there is one state where both are folded, one where both are ruptured, and two where one is folded and one is ruptured; when $N = 3$, there is one state where all are folded, one where all are ruptured, three where one is ruptured, and three where two are ruptured; and so on. To simulate T_{tol} for a given mMTP and (θ, ϕ) pair, we consider an ensemble of identical mMTPs exposed to the same force, and define the fraction of sensors in each state using a fraction vector $\boldsymbol{f} = [f_1, f_2, \ldots, f_j, \ldots, f_{2^N}]$, where f_j denotes the fraction of probes in the jth state.

The transitions between states result from force-dependent rupturing of force-sensitive units. For a TGT, the kinetic rate constant for bond rupture for the ith force-sensitive unit (denoted $k_{\text{rup},i}$) can be represented using the Bell model:

$$k_{\text{rup},i} = k_0\,\exp\left(\frac{G_{\text{stretch},i}}{G^*}\right), \tag{3}$$

where $k_0 \approx 10^{-6}$ s^{-1} is the zero-force off rate of the duplex [41] and G^* is a characteristic constant specific to each type of probe. For the low-force (unzip) and high-force (shear) TGTs we used $G^* = 0.525$ and 1.66 because these values produced $T_{\text{tol}} = 12$ pN and 56 pN respectively when $N = 1$.

In order to determine T_{tol} for a given set of θ, ϕ, N, and G^* parameters, we implemented the following algorithm in MATLAB:

(a) Set $|\boldsymbol{F}| = 0.1$ pN
(b) For each possible state, calculate $\boldsymbol{R}$ and the $G_{\text{stretch},i}$ values using the fmincon function. From $G_{\text{stretch},i}$, calculate $k_{\text{rup},i}$. Use these values to construct a Markov transition matrix ($\boldsymbol{M}$) with a timestep $\Delta t = 0.0001$ s.
(c) Initialize the fraction vectors with $f_1 = 1$ and $f_j = 0$ for all $j > 1$.

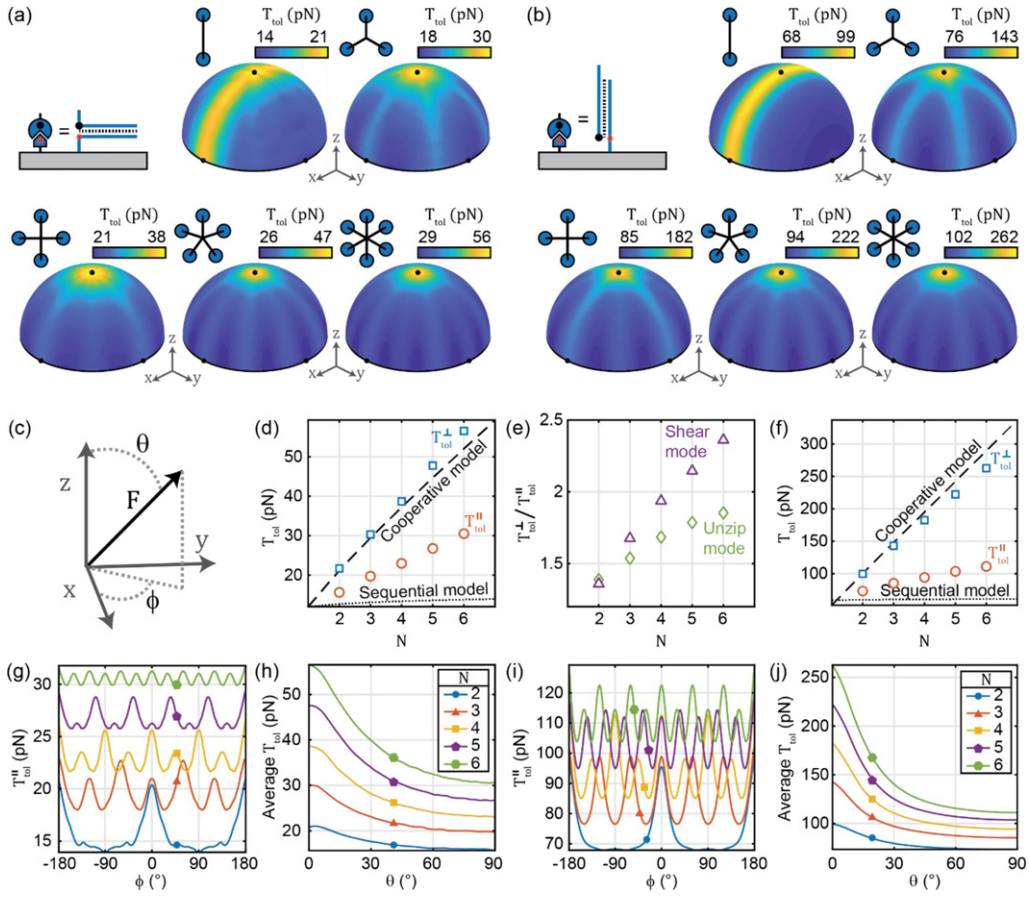

Figure 2. Results of simulations of mMTPs with $2 \leqslant N \leqslant 6$ low or high force TGTs. (a) Simulation results of low-force (unzipping-mode TGTs) mMTPs. Five T_{tol} maps are shown with the geometry of the corresponding mMTP shown above the map and to the left. Each map is a hemisphere with black dot showing the points where the x-, y-, and z-axes intersect with the hemisphere, as well as a black circle showing the intersection between the hemisphere and the x–y plane. The color of each point on the map denotes the simulated T_{tol} of the mMTP when pulled with a force vector that is coincident with the point. Each map's colorbar is labeled with the minimum and maximum recorded T_{tol}, rounded to the nearest integer. (b) Same as in subfigure (a), but for mMTPs with high force (shearing mode) TGTs. (c) Coordinate system showing tilt angle (θ) and azimuthal angle (ϕ) used in this work. (d) Plot of $T_{tol}^{\perp}$ (blue squares) and $T_{tol}^{\parallel}$ (orange circles) as a function of N for the mMTPs with low-force TGTs. For reference, the cooperative and sequential rupture models developed by Williams are shown as dashed and dotted lines, respectively. (e) The ratio $T_{tol}^{\perp}/T_{tol}^{\parallel}$ as a function of N for mMTPs with low force (purple triangles) and high force (green diamonds) TGTs. (f) Same as in subfigure (d), but for mMTPs with high force TGTs. (g) T_{tol} as a function of ϕ when $\theta = 90°$ for mMTPs with low-force TGTs. (h) T_{tol} averaged across all ϕ as a function of θ. (i) and (j) Same as in subfigures (g) and (h), but for mMTPs with high force TGTs. ** Suggestion to swap (g) and (h) so that phi plot next to each other and theta plots next to each other. This way the legend would appear first and then you can lump the ϕ plots together.

(d) Apply a timecourse to the fraction vector through matrix multiplication:

$$f := \boldsymbol{M}^{p} f, \tag{4}$$

where $p = t_{obs}/\Delta t = 10\,000$ for calculations of T_{tol}.

(e) Check if $f_{2N} < 0.5$. If so, increment $|\boldsymbol{F}|$ by 0.1 pN and repeat steps 2–5.

(f) If $f_{2N} \geqslant 0.5$, then at least half of the probes are fully opened. At this point, T_{tol} is calculated by interpolating between the f_{2N} values calculated at the current and previous $|\boldsymbol{F}|$ levels to estimate the force that results in $f_{2N} = 0.5$.

We repeated these calculations for a representative set of (θ, ϕ) combinations. Specifically, we tested combinations of θ values ranging from 0 to $\pi/2$ and ϕ values ranging from 0 to $\pi/(N+1)$ which, due to periodicity in the set of anchor points, is equivalent to testing all orientations with non-negative z-components. We repeated this analysis for various types of probes with various N values.

To compare the extreme cases of forces that are perpendicular and parallel to the surface, we define $T_{tol}^{\parallel}$ (for when $\theta = 90°$, which is calculated by averaging T_{tol} across all ϕ when $\theta = 90°$) and $T_{tol}^{\perp}$ (for $\theta = 0°$). We also define a ratio parameter ($T_{tol}^{\perp}/T_{tol}^{\parallel}$) to assess the extent to which the mMTP's force response is anisotropic.

To complete our analysis, we simulated mixed-mMTPs with various combinations of low- and high-force TGTs. In total we simulated 24 mixed-mMTPs (1 with $N = 2$, 2 with $N = 3$, 4 with $N = 4$, 6 with $N = 5$, and 11 with $N = 6$), representing all possible

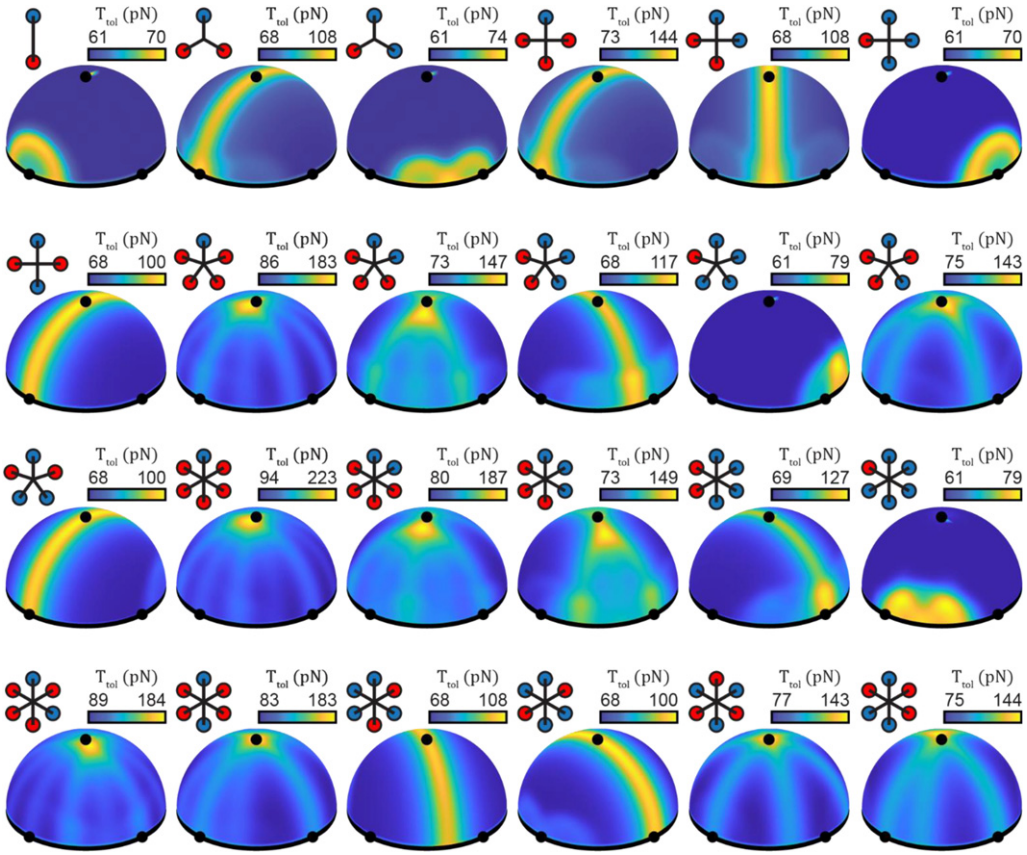

Figure 3. T_{tol} maps, as originally depicted in figures 2(a) and (b), are shown for all 24 possible mixed-mMTP designs investigated in this work. The geometry of each design above and to the left of each hemispherical T_{tol} map. In these representations, high-force TGTs are depicted as red circles and low-force TGTs are depicted as blue circles.

geometries when removing designs that are redundant due to symmetry. For these simulations, we simulated ϕ values ranging from 0 to 2π because periodic symmetry is no longer necessarily maintained.

3. Results

We started by simulating T_{tol} for an mMTP with $N = 3$ low force TGTs. As expected, T_{tol} shows a substantial orientation-dependence that ranges from $T_{tol}^{\perp} = 20.2$ pN when $\theta = 0°$ to 14.1 pN when $\theta = 90°$. Averaging across all ϕ values with $\theta = 90°$ reveals that $T_{tol}^{\parallel} = 15.1$ pN. As such, we found that $T_{tol}^{\perp}/T_{tol}^{\parallel} = 1.41$. Setting $\theta = 90°$, caused force to concentrate onto one or two of the springs, resulting in a low degree of cooperativity that ultimately led to sequential bond rupture. In contrast, setting $\theta = 0°$ resulted in equal distribution of load to all three TGTs, which led to cooperative bond rupture at higher $\boldsymbol{F}$.

We next repeated these simulations using N values ranging from 2 to 6 (figures 2(a) and (b)), and found that $T_{tol}^{\parallel}$ and $T_{tol}^{\perp}$ both increased monotonically with N (figures 2(d) and (f)). $T_{tol}^{\perp}$ increased according to the parallel bond rupture model (cooperative model) presented by Williams [39], which maximizes the scaling between T_{tol} and N. $T_{tol}^{\parallel}$ increased in a fashion that more closely resembled the sequential bond rupture model (also presented by Williams [39]), which minimizes the scaling between T_{tol} and N due to poor cooperativity between multiple force sensitive units (figures 2(d) and (f)).

The ratio $T_{tol}^{\perp}/T_{tol}^{\parallel}$ increased monotonically with N to a maximum of 1.85 and 2.36 for the low and high-force probes, respectively (figure 2(e)). Furthermore, both types of probes exhibited trends that suggest that increasing N further would result in further increases in $T_{tol}^{\perp}/T_{tol}^{\parallel}$.

Both classes of mMTPs (high- and low-force TGTs) exhibited notable ϕ-dependence of T_{tol} in a manner that reflected the geometry of the probes. The $N = 2$ probes exhibited a high-T_{tol} 'stripe' (figures 2(a) and (b)) corresponding to the plane normal to the axis connecting the two TGTs' anchor points. When $N \geqslant 3$ the highest T_{tol} was recorded in a single central node at $\theta = 0°$ with mild ϕ-dependent T_{tol} variations when $\theta \gg 0°$ (figures 2(g) and (i)). As N increased, the dependence of T_{tol} on ϕ decreased (figures 2(g) and (i)).

When averaging with respect to ϕ all probes exhibited monotonically-decreasing T_{tol} that decreased in a decaying exponential fashion (figures 2(h) and (j)). Together, these results suggest that higher values of N may be preferable when the intended task is to achieve θ-dependent anisotropic mechanosensing.

We observed several notable differences between the mMTPs with low-force TGTs and the mMTPs with high-force TGTs. The mMTPs with high-force TGTs appeared to exhibit a more rapid decay in T_{tol} with respect to θ (figures 2(h) and (j)), as well as larger periodic variations (both in absolute and relative terms) with respect to ϕ (figures 2(g) and (i)). The ratio $T_{tol}^{\perp}/T_{tol}^{\parallel}$ increased more steeply with N for the mMTPs with high-force TGTs (figure 2(e)), which appeared to be largely due to high-force mMTP's higher adherence to the sequential bond rupture model at high θ (figure 2(f)) than the low-force mMTPs (figure 2(d)).

We speculate that most of these differences arise largely due to the difference in w between the two types of TGTs (4.6 nm for the low force TGT and 8.7 nm for the high force TGT). Higher w should result in less cooperativity between the TGTs when $\theta > 0°$, which will result in a lower T_{tol} relative to $T_{tol}^{\perp}$. This last point is evident when considering the limiting case of $w = 0$, wherein all force orientations will result in equal cooperativity and thus equal T_{tol}. Higher w may also slightly reduce $T_{tol}^{\perp}$ by imposing small pre-stresses that reduce the amount of externally-applied force required to rupture the TGTs (figure 2(f)), but this effect appears to be minimal.

We next performed simulations of mixed-mMTPs (figure 3) with combinations of high-force and low-force TGTs. With a few exceptions, we found that the T_{tol} pattern was generally dependent on the number of high-force TGTs. Designs with one high-force TGT exhibited a new pattern unique to the mixed designs, wherein a single high-T_{tol}, high-θ node sits opposite the high force TGT's anchor point. This pulling geometry appears to produce increased T_{tol} because force is highly concentrated on the single high-force TGT yet a small amount of force (too small to drive rupture) is borne by the low-force TGTs, thus resulting in a 10–20 pN enhancement in T_{tol}. Designs with two high-force TGTs exhibited a stripe of high T_{tol}, similar to the pattern for the $N = 2$ designs described above. Designs with 3 or more high-force TGTs exhibited nodes at or near $\theta = 0°$ similar to the non-mixed probes with $N \geqslant 3$. None of the mixed-mMTP designed produced $T_{tol}^{\perp}/T_{tol}^{\parallel}$ ratios surpassing the mMTP with $N = 6$ high-force TGTs. Together, these results suggest that mixed mMTPs may be useful for engineering both θ- and ϕ-dependence.

4. Discussion

Our simulation results suggest that mMTPs may be viable as synthetic anisotropic mechanosensors. Currently, MTP-based studies of the role of anisotropic mechanosensation can be performed by using supported lipid bilayers to completely eliminate resistence to lateral force [3, 42]. mMTPs may provide a complementary approach that could better mimic biological scenarios, wherein cells perform anisotropic mechanosensation on ligands that are bound to the extracellular matrix.

However, there are practical concerns associated with experimental implementation of mMTPs. Here, we briefly consider aspects of mMTP design, synthesis, surface attachment, and interpretation that may have important practical implications.

mMTP synthesis will require a body that can couple with multiple MTPs as well as a ligand such as cyclic arginine–glycine–asparagine (cRGD—an integrin-binding peptide). One strategy to form an $N = 3$ mMTP could be to use the protein streptavidin, which can form high-affinity bonds with up to four biotin molecules simultaneously, as the mMTP body. Mixing streptavidin with a molar excess of biotin-capped MTPs will result primarily in streptavidin molecules that are bound to either 3 or 4 MTPs. Native gel-based purification could be used to separate out the $N = 3$ subset, which could then be incubated with biotin-cRGD to form mMTPs with $N = 3$. Chemical groups such as alkynes or thiols at the bottom termini of the constituent MTPs could then be used to link the mMTPs to a glass coverslip for cellular studies. However, the biotin–streptavidin bond is also subject to force-dependent rupture [11] such that, when $T_{tol}^{\perp}$ is high (e.g. for high-force TGTs) the cRGD-biotin–streptavidin bond may rupture before cooperative rupture of the MTPs. Accordingly, mMTPs with higher force thresholds or with $N > 3$ will require alternative approaches, such as covalent conjugation [43] to a small molecule body with $N + 1$ functional groups.

Using simulations, we have considered ideal scenarios wherein mMTP anchor points are uniformly distributed around a central point. In reality, mMTPs will exhibit deviations from this behavior that will result in force loading that is not fully cooperative, even when $\theta = 0°$. Furthermore, some fraction of mMTPs will inevitably be defective, with $< N$ MTPs properly anchored to the underlying substrate. The quantification of the effects of these factors using computational and/or experimental methods will be critical for correct interpretation of experimental data.

A potentially problematic aspect of our approach is that increasing $T_{tol}^{\perp}/T_{tol}^{\parallel}$ also increased $T_{tol}^{\perp}$ in all cases simulated. The study of anisotropic mechanosensors that operate in relatively low force ranges (for example, $CD8^{+}$ mouse T cells transmit force in the 12–19 pN range through their TCRs [25, 34, 44]) may require alternative designs. One potential solution is to use mMTPs with very low force TGTs that use nucleosome unwrapping [45], rather than duplex rupture, as the force dependent process to achieve $T_{tol} = 4$ pN. Our simulations are also limited in their method of calculating T_{tol}; we

assumed that forces applied to mMTPs were time-invarient, but in biologically-relevant contexts force are dynamic. In future work, it may be necessary to investigate the dependence of T_{tol} for mMTPs on force loading rate. However, we expect that the general trends observed in this work will remain unchanged.

Another trend that could be investigated in future work is the effect of spacer length on $T_{tol}^{\perp}/T_{tol}^{\parallel}$. Generally, we expect $T_{tol}^{\perp}/T_{tol}^{\parallel}$ to correlate with $w/|\boldsymbol{R}|$. For mMTPs with unzipping mode TGTs, w would approach zero as spacer length approached zero, while for shear-mode mMTPs w would approach the length of the TGTs' DNA duplexes. For long spacer lengths, we expect that w would increase sub-linearly with spacer length (due to the inherent characteristics of WLCs) while $|\boldsymbol{R}|$ would approach linear scaling with increasing spacer length. Therefore, we expect that $T_{tol}^{\perp}/T_{tol}^{\parallel}$ may exhibit a nonzero maximum for mMTPs with unzipping-mode TGTs and decrease monotonically for mMTPs with shear mode TGTs.

In conclusion, mMTPs are promising examples of synthetic anisotropic mechanosensors. Our simulations demonstrate how multivalency can be used to engineer anisotropic mechanosensation *de novo*. In future works, we aim to develop mMTPs and leverage them to reveal unique properties of receptors such as the TCR and integrins, and to reveal fundamental biophysical aspects of receptor–ligand interactions.

Acknowledgments

This work was supported through National Science Foundation IDBR 1353939 (KS), National Institute of General Medical Sciences (NIGMS) RO1 GM124472 (KS), NSF 1350829 (KS), and NSF GRFP DGE-1444932 (ATB).

ORCID iDs

Aaron T Blanchard https://orcid.org/0000-0002-3129-6591
Khalid Salaita https://orcid.org/0000-0003-4138-3477

References

[1] Chen Y, Ju L, Rushdi M, Ge C and Zhu C 2017 Receptor-mediated cell mechanosensing *Mol. Biol. Cell* **28** 3134–55
[2] Kim S T, Takeuchi K, Sun Z-Y J, Touma M, Castro C E, Fahmy A, Lang M J, Wagner G and Reinherz E L 2009 The $\alpha\beta$ T cell receptor is an anisotropic mechanosensor *J. Biol. Chem.* **284** 31028–37
[3] Zhang Y, Qiu Y, Blanchard A T, Chang Y, Brockman J M, Ma V P, Lam W A and Salaita K 2017 Platelet integrins exhibit anisotropic mechanosensing and harness piconewton forces to mediate platelet aggregation *Proc. Natl Acad. Sci. USA* **115** 325–30
[4] Brockman J M and Salaita K 2019 Mechanical proofreading: a general mechanism to enhance the fidelity of information transfer between cells *Front. Phys.* **7** 14
[5] Huang D L, Bax N A, Buckley C D, Weis W I and Dunn A R 2017 Vinculin forms a directionally asymmetric catch bond with F-actin *Science* **357** 703
[6] Neuman K C and Nagy A 2008 Single-molecule force spectroscopy: optical tweezers, magnetic tweezers and atomic force microscopy *Nat. Methods* **5** 491–505
[7] Stabley D R, Jurchenko C, Marshall S S and Salaita K S 2011 Visualizing mechanical tension across membrane receptors with a fluorescent sensor *Nat. Methods* **9** 64–7
[8] Liu Y, Yehl K, Narui Y and Salaita K 2013 Tension sensing nanoparticles for mechano-imaging at the living/nonliving interface *J. Am. Chem. Soc.* **135** 5320–3
[9] Galior K, Liu Y, Yehl K, Vivek S and Salaita K 2016 Titin-based nanoparticle tension sensors map high-magnitude integrin forces within focal adhesions *Nano Lett.* **16** 341–8
[10] Morimatsu M, Mekhdjian A H, Adhikari A S and Dunn A R 2013 Molecular tension sensors report forces generated by single integrin molecules in living cells *Nano Lett.* **13** 3985–9
[11] Jurchenko C, Chang Y, Narui Y, Zhang Y and Salaita K S 2014 Integrin-generated forces lead to streptavidin–biotin unbinding in cellular adhesions *Biophys. J.* **106** 1436–46
[12] Chang Y, Liu Z, Zhang Y, Galior K, Yang J and Salaita K 2016 A general approach for generating fluorescent probes to visualize piconewton forces at the cell surface *J. Am. Chem. Soc.* **138** 2901–4
[13] Zhang Y, Ge C, Zhu C and Salaita K 2014 DNA-based digital tension probes reveal integrin forces during early cell adhesion *Nat. Commun.* **5** 5167
[14] Blanchard A T and Salaita K 2019 Emerging uses of DNA mechanical devices *Science* **365** 1080–1
[15] Blanchard A T, Bazrafshan A S, Yi J, Eisman J T, Yehl K M, Bian T, Mugler A and Salaita K 2019 Highly polyvalent DNA motors generate 100+ pN of force via autochemophoresis *Nano Lett.* **19** 6977–86
[16] Su H, Liu Z, Liu Y, Ma V P-Y, Blanchard A, Zhao J, Galior K, Dyer R B and Salaita K 2018 Light-responsive polymer particles as force clamps for the mechanical unfolding of target molecules *Nano Lett.* **18** 2630–6
[17] Bazrafshan A, Meyer T A, Su H, Brockman J M, Blanchard A T, Piranej S, Duan Y, Ke Y and Salaita K 2020 Tunable DNA origami motors translocate ballistically over μm distances at nm/s speeds *Angew. Chem., Int. Ed.* **59** 9514–21
[18] Wang X and Ha T 2013 Defining single molecular forces required to activate integrin and notch signaling *Science* **340** 991
[19] Wang X, Rahil Z, Li I T S, Chowdhury F, Leckband D E, Chemla Y R and Ha T 2016 Constructing modular and universal single molecule tension sensor using protein *G* to study mechano-sensitive receptors *Sci. Rep.* **6** 21584
[20] Wang Y, LeVine D N, Gannon M, Zhao Y, Sarkar A, Hoch B and Wang X 2018 Force-activatable biosensor enables single platelet force mapping directly by fluorescence imaging *Biosens. Bioelectron.* **100** 192–200
[21] Wang X, Sun J, Xu Q, Chowdhury F, Roein-Peikar M, Wang Y and Ha T 2015 Integrin molecular tension within motile focal adhesions *Biophys. J.* **109** 2259–67
[22] Wang Y and Wang X 2016 Integrins outside focal adhesions transmit tensions during stable cell adhesion *Sci. Rep.* **6** 36959
[23] Chowdhury F *et al* 2015 Single molecular force across single integrins dictates cell spreading *Integr. Biol.* **7** 1265–71
[24] Roein-Peikar M, Xu Q, Wang X and Ha T 2016 *Phys. Rev.* X **6** 011001
[25] Liu Y, Blanchfield L, Ma V P-Y, Andargachew R, Galior K, Liu Z, Evavold B and Salaita K 2016 DNA-based nanoparticle tension sensors reveal that T-cell receptors transmit defined pN forces to their antigens for enhanced fidelity *Proc. Natl Acad. Sci. USA* **113** 5610–5

[26] Rao T C, Ma V P-Y, Blanchard A, Urner T M, Grandhi S, Salaita K and Mattheyses A L 2020 EGFR activation attenuates the mechanical threshold for integrin tension and focal adhesion formation *J. Cell Sci.* **133** jcs238840
[27] Brockman J M *et al* 2020 *Nat. Methods* **17** 1018–24
[28] Ma V P-Y, Liu Y, Yehl K, Galior K, Zhang Y and Salaita K 2016 Mechanically induced catalytic amplification reaction for readout of receptor-mediated cellular forces *Angew. Chem., Int. Ed.* **55** 5488–92
[29] Zhao Y, Sarkar A and Wang X 2020 Peptide nucleic acid based tension sensor for cellular force imaging with strong DNase resistance *Biosens. Bioelectron.* **150** 111959
[30] Blakely B L *et al* 2014 A DNA-based molecular probe for optically reporting cellular traction forces *Nat. Methods* **11** 1229–32
[31] Brockman J M *et al* 2017 Mapping the 3D orientation of piconewton integrin traction forces *Nat. Methods* **15** 115
[32] Blanchard A T, Brockman J M, Salaita K and Mattheyses A L 2020 Variable incidence angle linear dichroism (VALiD): a technique for unique 3D orientation measurement of fluorescent ensembles *Opt. Express* **28** 10039–61
[33] Blanchard A T *et al* 2020 *Nat. Res.* (https://doi.org/10.21203/rs.3.rs-83810/v1)
[34] Ma R, Kellner A V, Ma V P-Y, Su H, Deal B R, Brockman J M and Salaita K 2019 DNA probes that store mechanical information reveal transient piconewton forces applied by T cells *Proc. Natl Acad. Sci. USA* **116** 16949
[35] Murad Y and Li I T S 2019 Quantifying molecular forces with serially connected force sensors *Biophys. J.* **116** 1282–91
[36] Baig M M F A, Zhang Q-W, Younis M R and Xia X-H 2019 A DNA nanodevice simultaneously activating the EGFR and integrin for enhancing cytoskeletal activity and cancer cell treatment *Nano Lett.* **19** 7503–13
[37] Zhao B, O'Brien C, Mudiyanselage A P K K K, Li N, Bagheri Y, Wu R, Sun Y and You M 2017 Visualizing intercellular tensile forces by DNA-based membrane molecular probes *J. Am. Chem. Soc.* **139** 18182–5
[38] Dutta P K, Zhang Y, Blanchard A T, Ge C, Rushdi M, Weiss K, Zhu C, Ke Y and Salaita K 2018 Programmable multivalent DNA-origami tension probes for reporting cellular traction forces *Nano Lett.* **18** 4803–11
[39] Williams P M 2003 Analytical descriptions of dynamic force spectroscopy: behaviour of multiple connections *Anal. Chim. Acta* **479** 107–15
[40] Petrosyan R 2017 Improved approximations for some polymer extension models *Rheol. Acta* **56** 21–6
[41] Mosayebi M, Louis A A, Doye J P K and Ouldridge T E 2015 Force-induced rupture of a DNA duplex: from fundamentals to force sensors *ACS Nano* **9** 11993–2003
[42] Glazier R, Brockman J M, Bartle E, Mattheyses A L, Destaing O and Salaita K 2019 DNA mechanotechnology reveals that integrin receptors apply pN forces in podosomes on fluid substrates *Nat. Commun.* **10** 4507
[43] Ma V P-Y *et al Proc. Natl Acad. Sci.* in review (submitted)
[44] Ma V P-Y, Liu Y, Blanchfield L, Su H, Evavold B D and Salaita K 2016 Ratiometric tension probes for mapping receptor forces and clustering at intermembrane junctions *Nano Lett.* **16** 4552–9
[45] Chowdhury F *et al* 2016 Defining single molecular forces required for notch activation using nano yoyo *Nano Lett.* **16** 3892–7